Simulation Analysis of Conduction Block in Unmyelinated Axons Induced by High-Frequency Biphasic Electrical Currents

Changfeng Tai, *Senior Member, IEEE*, William C. de Groat, and James R. Roppolo

***Abstract*—Nerve conduction block induced by high-frequency biphasic electrical currents is analyzed using a lumped circuit model of the unmyelinated axon based on Hodgkin-Huxley equations. Axons of different diameters (5–20 μm) can not be blocked completely when the stimulation frequency is between 2 kHz and 4 kHz. However, when the stimulation frequency is above 4 kHz, all axons can be blocked. At high-frequency a higher stimulation intensity is needed to block nerve conduction. The larger diameter axon has a lower threshold intensity for conduction block. The stimulation waveform in which the pulsewidth changes with frequency is more effective in blocking nerve conduction than the waveform in which the pulsewidth is fixed. The activation of potassium channels, rather than inactivation of sodium channels, is the possible mechanism underlying the nerve conduction block of the unmyelinated axon. This simulation study further increases our understanding of axonal conduction block induced by high-frequency biphasic currents, and can guide future animal experiments as well as optimize stimulation waveforms that might be used for electrical nerve block in clinical applications.**

***Index Terms*—Axon, electrical stimulation, high-frequency, nerve block, model.**

I. Introduction

A REVERSIBLE peripheral nerve block would be of great value in clinical applications. For example, blocking pudendal nerve conduction during micturition could reduce urethral pressure and improve voiding efficiency for spinal cord injured patients [1]–[3]. Nerve block might also be used to treat chronic pain originating from a site of peripheral nerve injury [4], [5]. Blocking nerve conduction gradually beginning with larger fibers and then extending to smaller fibers as blocking intensity is increased [6]–[8] could be applied in functional neuromuscular stimulation to activate muscles in a physiological recruitment order and reduce muscle fatigue. Understanding the biophysics of nerve conduction block induced by electrical currents will be very helpful in developing new methods to block peripheral nerves under different clinical conditions.

In chronic applications, biphasic stimulation causes less tissue damage due to electro-chemical reactions than uniphasic stimulation [9]. Therefore, a method employing biphasic electrical currents to block nerve conduction will be very attractive. Animal experiments showed that high-frequency biphasic electrical currents applied to peripheral nerves could block conduction of action potentials [10]–[14]. This nerve block was quickly reversible once the stimulation was removed. However, the mechanism of nerve conduction block induced by high-frequency biphasic electrical currents is unknown. Since the biphasic electrical currents can depolarize and hyperpolarize the nerve membrane alternatively, it can not be assumed that the block is due to either membrane depolarization or hyperpolarization.

After Hodgkin and Huxley [15] successfully modeled the nerve membrane dynamics (HH model) based on experiments using squid giant unmyelinated axons, Frankenhaeuser and Huxley (FH model) [16] described the equations governing the myelinated nerve membrane dynamics based on experiments using frog nerves. In the following years, nerve membranes of mammalian myelinated axons were modeled using rabbits [17], and rats [18]. In 1976, McNeal [19] first modeled axons using many small axon segments described by the FH model and then

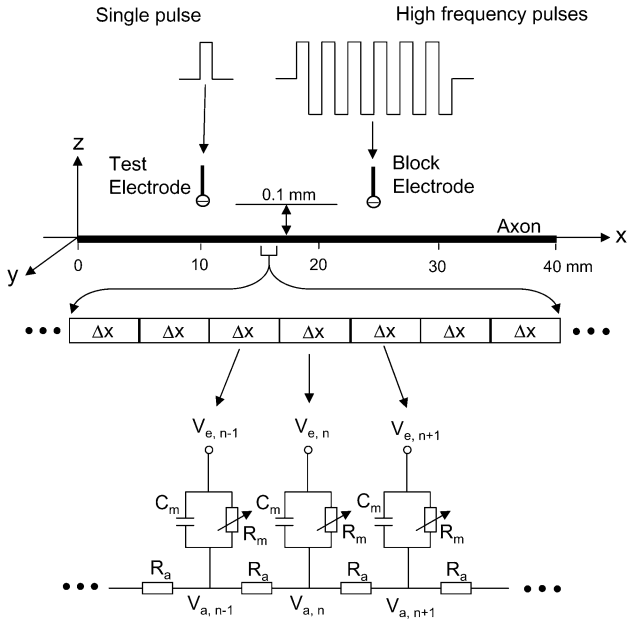

Fig. 1. Axon model to simulate conduction block by high-frequency biphasic pulses. The unmyelinated axon is segmented into many small cylinders of length Δx, each of which is modeled by a resistance-capacity circuit based on the Hodgkin-Huxley model. R_a : axoplasm resistance; R_m: membrane resistance; C_m: membrane capacitance; V_a: intracellular potential; V_e: extracellular potential.

Manuscript received May 14, 2004; revised December 23, 2004. This work is supported by the National Institutes of Health (NIH) under Grant 1R01-DK-068 566-01, Grant 1R01-NS-045 078-01, and Grant 1P01-HD-39 768-02. *Asterisk indicates corresponding author.*

*C. Tai is with the Department of Pharmacology, University of Pittsburgh, W1354 Biomedical Science Tower, Pittsburgh, PA 15261 USA (e-mail: cftai@pitt.edu).

W. de Groat and J. Roppolo are with the Department of Pharmacology, University of Pittsburgh, Pittsburgh, PA 15261 USA

Digital Object Identifier 10.1109/TBME.2005.847561

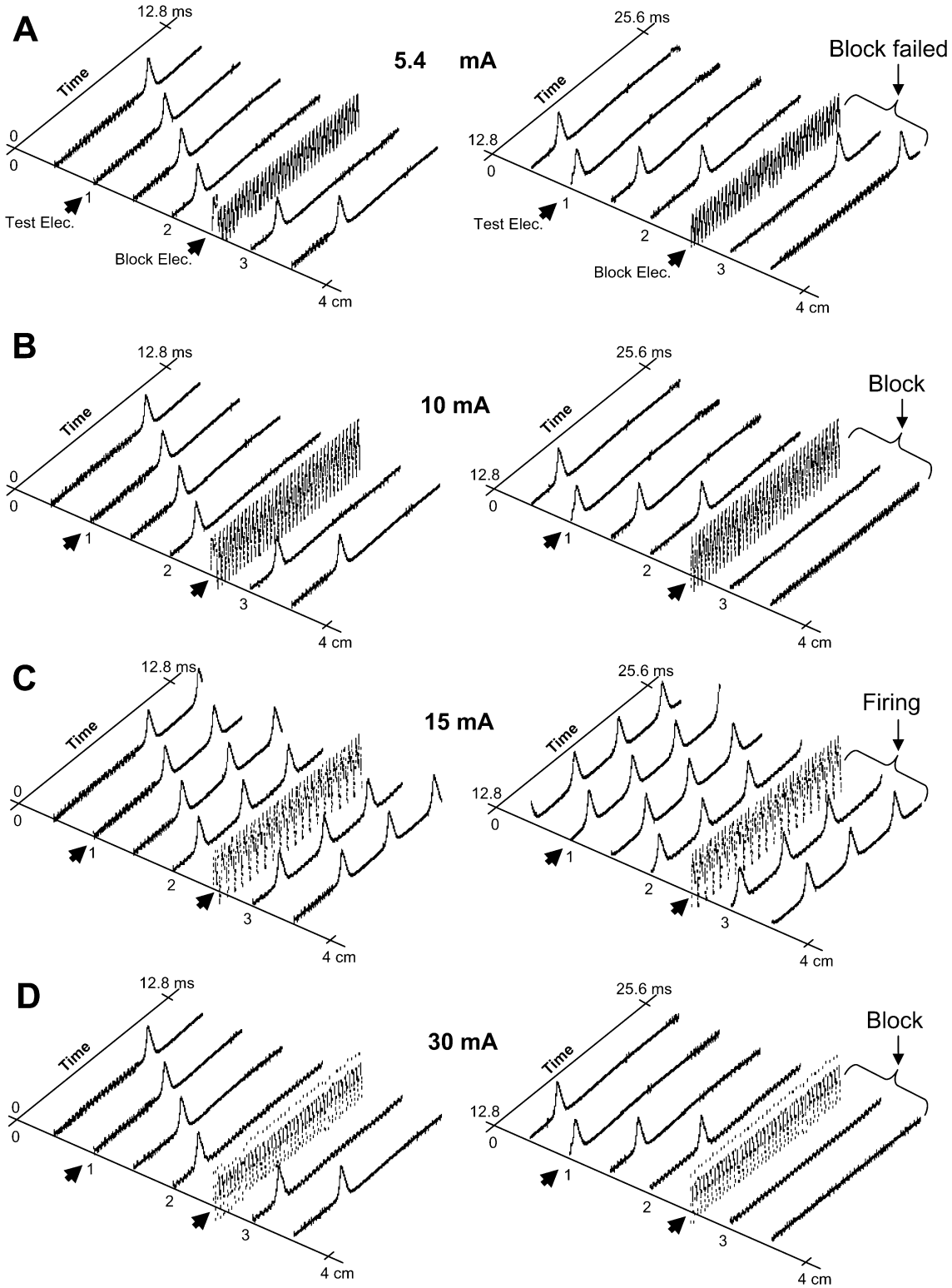

Fig. 2. The propagation of action potentials along the nerve generated by high-frequency biphasic pulses at different intensities: (A) 5.4 mA, (B) 10 mA, (C) 15 mA, and (D) 30 mA. Figures in the second column are continuations in time of the first column. An action potential is initiated by the test electrode at 12.8 ms as shown in (A), (B), and (D). The short arrows on every figures marked the locations for test and block electrodes. Stimulation frequency: 3.125 kHz. Axon diameter: 10 μm.

connecting them together with the resistances of the axoplasm. Since then many investigators [8], [20]–[26] have used this lumped circuit model, or sometimes more detailed models, with data from HH, FH or mammalian axon membranes to simulate and predict the nerve response to extracellular electrical stimulation. Most of these simulation studies focused on nerve excitation using low stimulation frequencies (below 1000 Hz). A few simulation studies [20], [21] explored high-frequency biphasic stimulation (up to 100 kHz), but they only investigated the nerve excitation rather than block. A theoretical analysis of nerve conduction block induced by high-frequency biphasic currents is not available.

In this paper, we analyzed the nerve conduction block induced by high-frequency biphasic current pulses using the lumped circuit model of unmyelinated axons based on HH equations. The purpose of this study is to evaluate the model's ability to simulate the known phenomena, predict unknown results and suggest possible mechanisms for the nerve block induced by high-frequency biphasic currents. Due to the unmyelinated axonal model, this study may be only applicable to the small C-fibers in mammalian nerves. Results from this simulation study could guide further experiments on animals, and optimize the stimulation waveforms to block peripheral nerve conduction.

II. Methods

The nerve model used in this study is shown in Fig. 1. A 40 mm long axon is segmented into many small cylinders of length $\Delta x = 0.5$ mm, each of which is modeled by a membrane capacitance and a variable membrane resistance. The ionic currents passing through the variable membrane resistance are described by Hodgkin-Huxley equations [15]. Two monopolar electrodes (with the indifferent electrode at infinity) are placed at 0.1 mm distance to the axon (Fig. 1). One is the block electrode at the 25 mm location along the axon, where the high-frequency biphasic current (as shown in Fig. 1) will be delivered. The other is the test electrode at the 10 mm location, which will deliver an uniphasic single pulse (pulse width: 0.1 ms; intensity: 2 mA) to evoke an action potential and test whether this action potential can propagate through the site of the block electrode. The test electrode will always be a cathode (negative pulse), and the block electrode will always deliver biphasic pulses with a cathodal pulse followed by a symmetric anodal pulse.

We assume that the axon is in an infinite homogeneous medium (resistivity $\rho_e = 300$ Ωcm). After neglecting the small influence induced by the presence of the axon in the homogeneous medium, the extracellular potential $V_{e,n}$ at the n th segment along the axon can be calculated by

$$V_{e,n}(t) = \frac{\rho_e}{4\pi}\left[\frac{I_{\text{block}}(t)}{\sqrt{(n\Delta x - x_0)^2 + z_0^2}} + \frac{I_{\text{test}}(t)}{\sqrt{(n\Delta x - x_1)^2 + z_1^2}}\right]$$

where $I_{\text{block}}(t)$ is the high-frequency biphasic current delivered to the block electrode (at location $x_0 = 25$ mm, $z_0 = 0.1$ mm); $I_{\text{test}}(t)$ is the single test pulse delivered to the test electrode (at location $x_1 = 10$ mm, $z_1 = 0.1$ mm).

The change of the membrane potential V_n at the n th segment is described by

$$\frac{dV_n}{dt} = \left[\frac{d}{4\rho_i}\left(\frac{V_{n-1} - 2V_n + V_{n+1}}{\Delta x^2} + \frac{V_{e,n-1} - 2V_{e,n} + V_{e,n+1}}{\Delta x^2}\right) - I_{i,n}\right] \Big/ c_m$$

where $V_n = V_{a,n} - V_{e,n} - V_{\text{rest}}$; $V_{a,n}$ is the intracellular potential at the n th segment; $V_{e,n}$ is the extracellular potential at the n th segment; V_{rest} is the resting membrane potential; d is the axon diameter; ρ_i is the resistivity of axoplasm (34.5 Ωcm); c_m is the capacity of the membrane (1 μF/cm^2); $I_{i,n}$ is the ionic current at the nth segment described by Hodgkin-Huxley equations (see Appendix) [15]. The model was solved by an implicit trapezoidal integration method with a time step of 0.01 ms [27]. The simulation always started at initial condition $V_n = 0$. The membrane potentials at the two end segments of the modeled axon were always equal to the membrane potentials of their closest neighbors, which implemented the sealed boundary conditions (no longitudinal currents) at the two ends of the modeled axon.

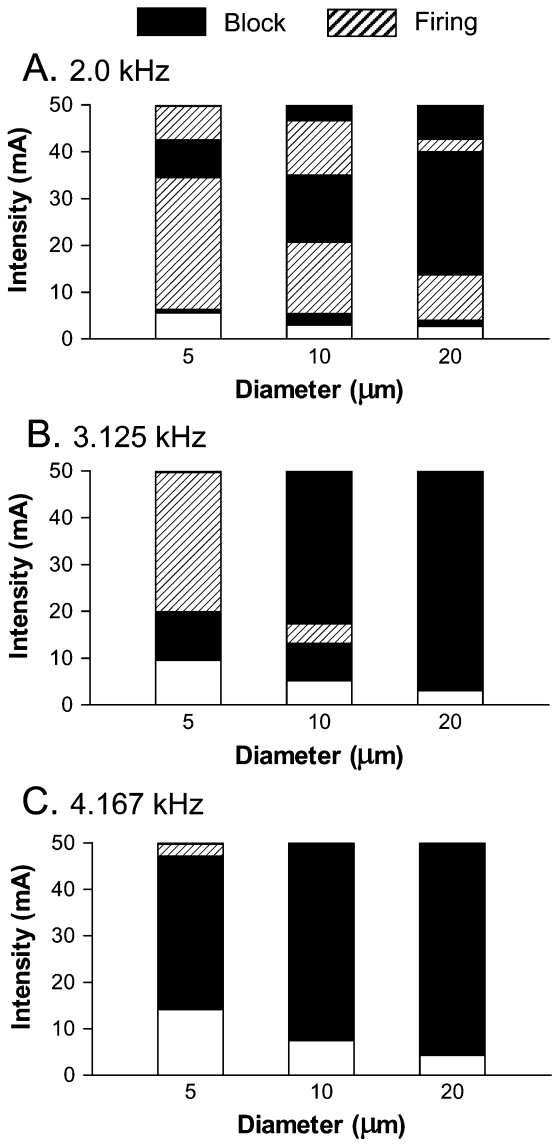

Fig. 3. Influence of stimulation frequency and axon diameter on nerve block when the frequency is below 4.167 kHz. The dark areas represent the stimulation intensity ranges causing nerve block. The hatched areas represent repetitive firing as shown in Fig. 2(C).

III. Results

A. Nerve Block With Stimulation Frequencies Below 4 kHz

Fig. 2 shows a typical nerve firing pattern and conduction block at different stimulation intensities when the frequency is below 4 kHz (3.12 kHz was used in Fig. 2). With the stimulation intensity below the block threshold as shown in Fig. 2(A), the

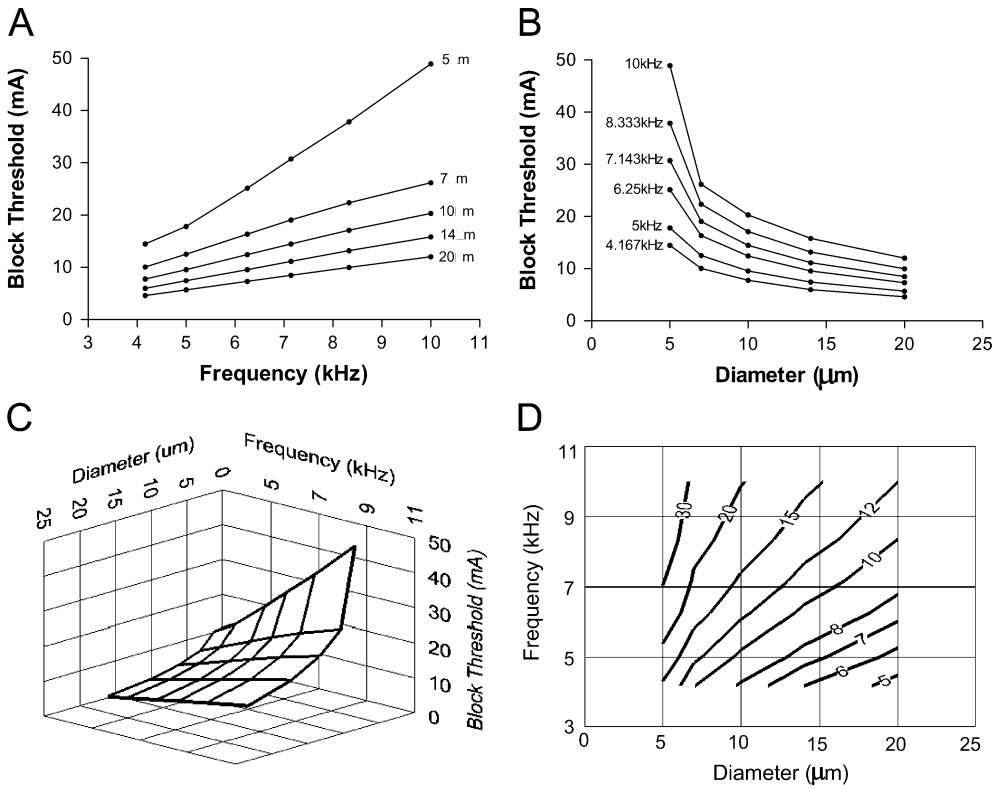

Fig. 4. Change of nerve block threshold with stimulation frequency and axon diameter when the frequency is above 4.167 kHz. (A) Block threshold changes with stimulation frequency for axons of different diameters. (B) Block threshold changes with axon diameter at different stimulation frequencies. (C) Block threshold changes with both stimulation frequency and axon diameter. (D) The maximum stimulation frequency can be used to block nerve axons larger than a certain diameter at different stimulation intensities. The numbers marked on each line in (D) indicate corresponding stimulation intensities in mA.

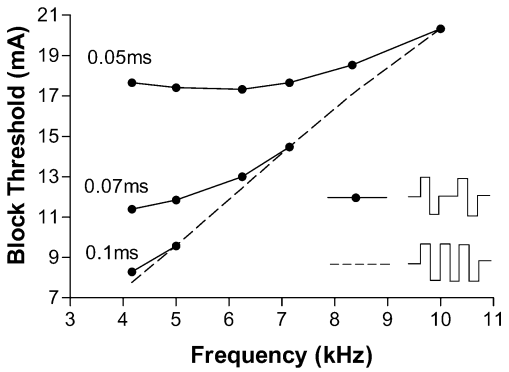

Fig. 5. Comparison of nerve block thresholds for stimulation with a fixed pulsewidth at different frequencies (solid lines) and for stimulation with the pulsewidth changing with stimulation frequency (dashed line). The numbers marked on each solid line indicate the corresponding fixed cathodal/anodal pulse width. Axon diameter: 10 μm.

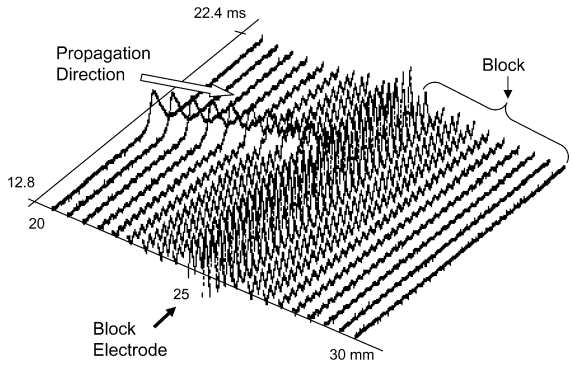

Fig. 6. A detailed presentation of nerve conduction block as shown in Fig. 2(B). Only the axon membrane activity within 5 mm distance to the high-frequency blocking electrode is shown during the time 12.8 ms to 22.4 ms. The propagated action potential is initiated by the test electrode at location 10 mm on the nerve as shown in Fig. 2(B).

action potential initiated by the test electrode (at location 1.0 cm and at time 12.8 ms) can still propagate through the site of the block electrode (at location 2.5 cm). However, propagation is blocked when the intensity of high-frequency stimulation is increased above the block threshold as shown in Fig. 2(B). However, further increasing the intensity of high-frequency stimulation causes repetitive firing as shown in Fig. 2(C), although the high-frequency stimulation only induces one action potential at other intensities [Fig. 2(A), (B), and (D)]. This repetitive firing disappears and nerve conduction can be blocked again if the stimulation intensity increases further [Fig. 2(D)].

The pattern of nerve firing and block changes with stimulation frequency and axon diameter (Fig. 3). At lower frequencies, nerves can fire repetitively over a larger range of stimulation intensities [Fig. 3(A)]. However, when frequency is increased above 4 kHz, the repetitive firing disappears and nerves can be blocked over a large range of intensities [Fig. 3(C)]. Fig. 3 also shows that the larger axons stop repetitive firing earlier than the smaller axons when the stimulation frequency is increased gradually. At frequencies below 4 kHz, there is only a very small range of stimulation intensities where a complete block of all nerve fibers with different diameters can occur [Fig. 3(A) and (B)].

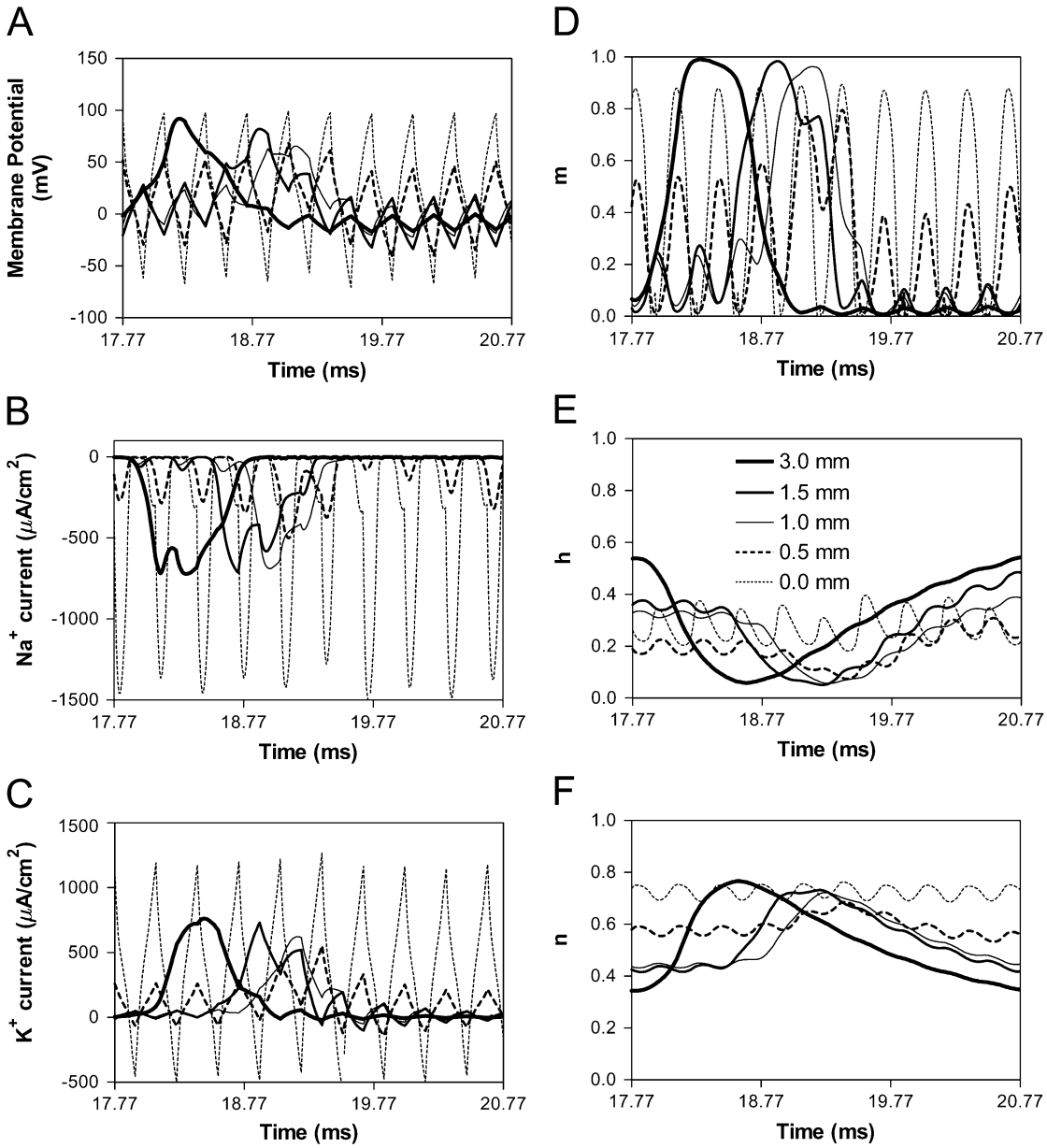

Fig. 7. Propagation of membrane potentials, ionic currents and activation/inactivation of the ion channels near the block electrode when nerve conduction block occurs as shown in Fig. 6. The legends in E are for all the figures, which indicate the distances to the block electrode (0.0 mm is right under the block electrode). m—activation of Na^+ channels; h—inactivation of Na^+ channels; n—activation of K^+ channels.

B. Nerve Block With Stimulation Frequencies Above 4 kHz

The threshold for nerve block changes with stimulation frequency and axon diameter when frequency is above 4 kHz (Fig. 4). Higher frequencies need higher stimulation intensities to block nerve conduction [Fig. 4(A)]. Larger diameter axons have lower block thresholds than smaller axons [Fig. 4(B)]. The changes in block thresholds with changes in both stimulation frequency and axon diameter are plotted as a surface in the frequency-diameter-threshold 3-D space in Fig. 4(C). Fig. 4(D) shows the contour lines of the threshold surface in Fig. 4(C) at different levels of stimulation intensity (numbers marked on lines are in units of mA). At a certain stimulation intensity [for example 12 mA in Fig. 4(D)], a higher frequency can only block the large axons. With frequency changing from high to low, more small axons can be blocked. If the stimulation intensity is too low, for example 7 mA in Fig. 4(D), axons of diameters smaller than 10 μm will never be blocked even with the lowest frequency of 4 kHz. There is a minimum stimulation intensity where it is possible to block the smallest axon with the lowest frequency [for example 15 mA in Fig. 4(D) to block 5-μm-diameter axon at frequency 4 kHz].

Stimulation with a fixed pulsewidth at different frequencies is less effective in blocking nerve conduction than that when the pulsewidth changes with frequency (Fig. 5). When 10 kHz stimulation (0.05 ms cathodal/anodal pulse width) is changed to 5 kHz, the pulsewidth is doubled if it changes with the frequency. This result also agrees with the finding that low frequencies are more effective than higher frequencies in blocking nerve conduction (Fig. 4), since the low frequency stimulation has a wider pulse width.

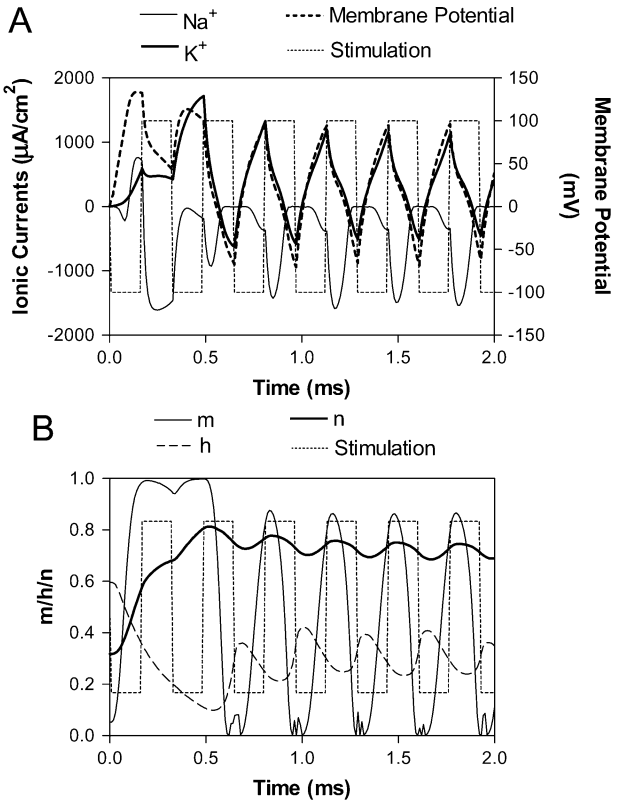

Fig. 8. Membrane potential, ionic currents, and activation/inactivation of the ion channels after the initial action potential as shown in Fig. 2(B). The stimulation waveform is re-scaled and plotted on the background to show the timing. m—activation of Na^+ channels; h—inactivation of Na^+ channels; n—activation of K^+ channels.

C. Mechanism of Nerve Conduction Block

The nerve conduction block in Fig. 2(B) occurs under the block electrode, which can be seen with a zoomed-in view in Fig. 6. The membrane potential oscillates (repetitively, depolarizing and hyperpolarizing) under the block electrode. The amplitude of this oscillating potential decreases rapidly within 2 mm distance (Fig. 6). Fig. 7 shows how membrane potentials, ionic currents, and activation/inactivation of the ion channels are gradually changed within a 3 mm distance to the block electrode in a short time scale (3 ms). The propagation of the action potential in terms of membrane potential [Fig. 7(A)], sodium [Fig. 7(B)], or potassium [Fig. 7(C)] currents can be detected within 0.5 mm distance of the block electrode, but it disappears under the block electrode (0.0 mm distance) where the membrane potential, and the sodium and potassium currents are oscillating. The activation (m) or inactivation (h) of sodium channels [Fig. 7(D) and (E)], and the activation (n) of potassium channels [Fig. 7(F)] are also changed gradually approaching the block electrode. At the location right under the block electrode, the activation (m) of sodium ion channels can still reach almost 0.9 during each stimulation pulse with its inactivation (h) oscillating around 0.3, which results in the pulsed inward sodium currents [Fig. 7(B)]. However, these inward sodium currents can not initiate action potentials because the activation (n) of potassium channels is increased to almost 0.8 and maintained at this level [Fig. 7(F)], which results in large outward potassium currents [Fig. 7(C)].

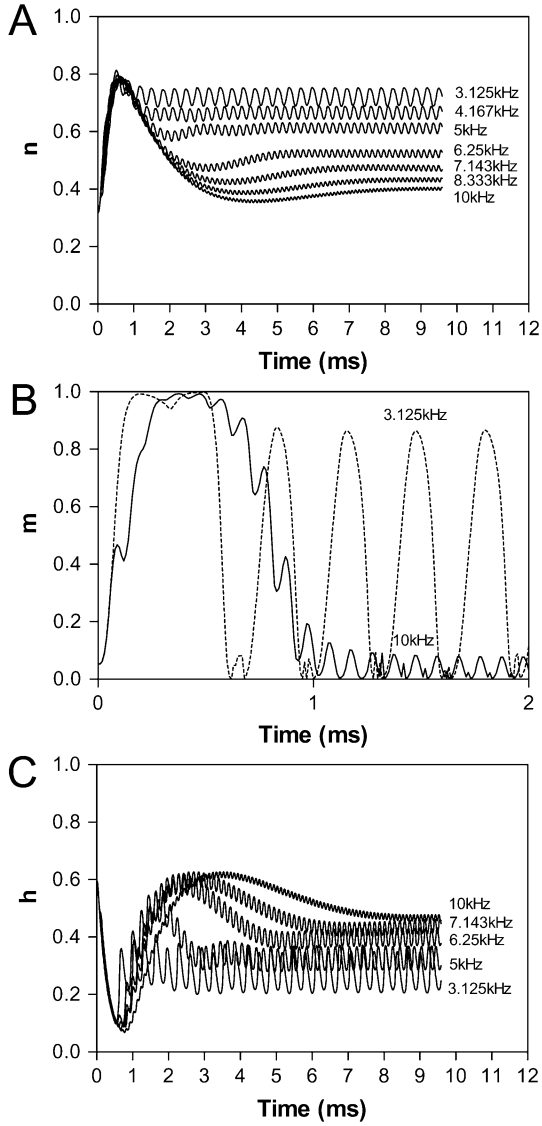

Fig. 9. Activation and inactivation of ion channels at different stimulation frequencies. (A) n—activation of K^+ channels. (B) m—activation of Na^+ channels. (C) h—inactivation of Na^+ channels. The frequencies marked on each figure are in the order of corresponding levels for activation or inactivation. Activation of Na^+ channels (m) is plotted only at two frequencies within a short time period for clarity. Stimulation intensity: 10 mA. Axon diameter: 10 μm.

Fig. 8 shows the membrane potential, ionic currents and activation/inactivation of the ion channels under the block electrode after the initial action potential as shown in Fig. 2(B). The stimulation waveform is re-scaled and plotted on the background to show the timing. After the initial action potential (less than 1 ms), the membrane falls into the same state as that shown in Fig. 7. The sodium current flows inward during each stimulus pulse, but initiation of action potentials fails due to the large outward potassium current [Fig. 8(A)]. The potassium current is tightly linked to the change of membrane potential [Fig. 8(A)] due to the constant activation of the potassium channels [Fig. 8(B)].

D. Activation and Inactivation of Ion Channels

Fig. 9 shows how the activation and inactivation of the ion channels under the block electrode change with stimulation frequency at a certain stimulation intensity (10 mA). A lower fre-

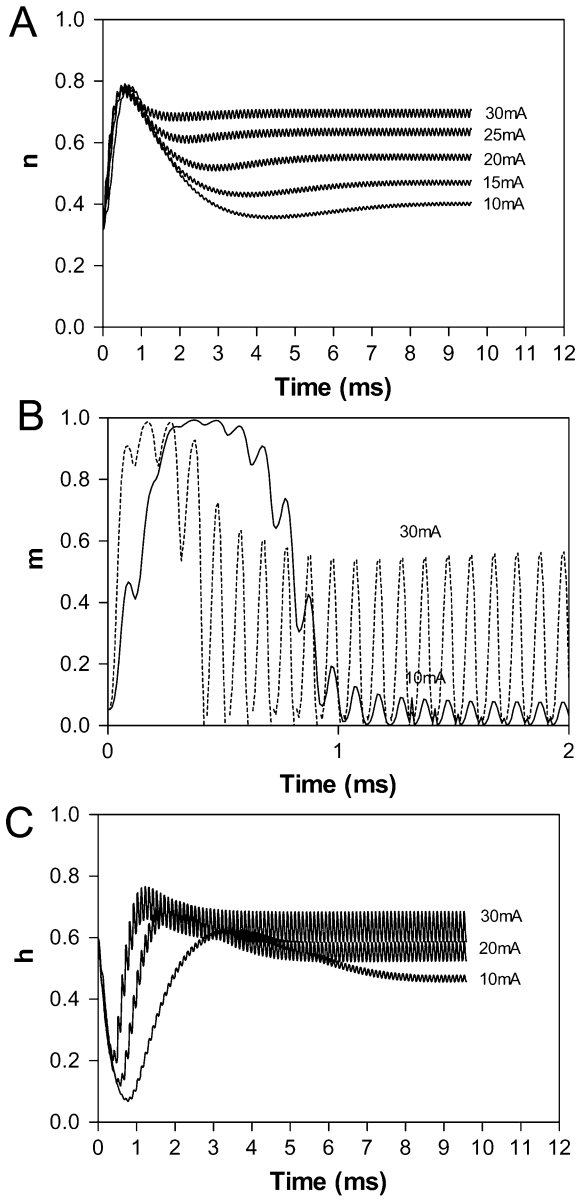

Fig. 10. Activation and inactivation of ion channels at different stimulation intensities. (A) n—activation of K^+ channels. (B) m—activation of Na^+ channels. (C) h—inactivation of Na^+ channels. The intensities marked on each figure are in the order of corresponding levels for activation or inactivation. Activation of Na^+ channels (m) is plotted only at two intensities within a short time period for clarity. Stimulation frequency: 10 kHz. Axon diameter: 10 μm.

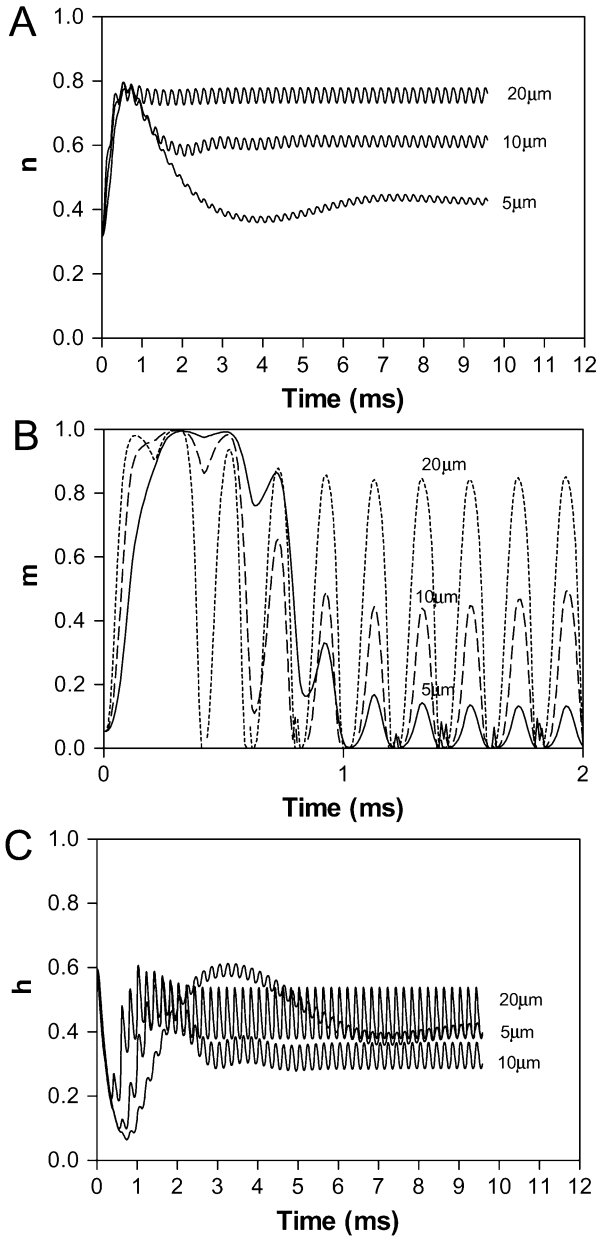

Fig. 11. Activation and inactivation of ion channels in different diameter axons. (A) n—activation of K^+ channels. (B) m—activation of Na^+ channels. (C) h—inactivation of Na^+ channels. The diameters marked on each figure are in the order of corresponding levels for activation or inactivation. Activation of Na^+ channels (m) is plotted only within a short time period for clarity. Stimulation frequency: 5 kHz. Stimulation intensity: 10 mA.

quency can maintain a higher activation level of potassium channels than a higher frequency [Fig. 9(A)], which explains why a lower stimulation frequency has a lower blocking threshold [Fig. 4(A)]. Although the lower frequency also increases activation of sodium channels [Fig. 9(B)] while moderately increasing the inactivation [Fig. 9(C)], it fails to generate action potentials due to the high activation level of potassium channels. The nerve conduction block occurs when the frequency is lower than 5 kHz (Fig. 9), which corresponds to the activation level of potassium channels at or above 0.6 [Fig. 9(A)].

Although the 10 kHz stimulation shown in Fig. 9 fails to block nerve conduction at 10 mA, it achieves nerve block with a higher intensity. Fig. 10 shows how the activation and inactivation of the ion channels under the block electrode change with stimulus intensity at a certain stimulation frequency (10 kHz). The 10-kHz stimulation blocks nerve conduction when the intensity is at 25 mA or above, which again corresponds to the activation level of potassium channels at or above 0.6 [Fig. 10(A)]. Although at a higher stimulation intensity the activation level of sodium channels is increased [Fig. 10(B)] in concert with a decrease in inactivation [Fig. 10(C)], nerve block can still be achieved due to the high activation level of potassium channels.

Fig. 11 shows how the activation and inactivation of the ion channels under the block electrode change with axon diameter at a certain stimulation frequency (5 kHz) and intensity (10 mA). The

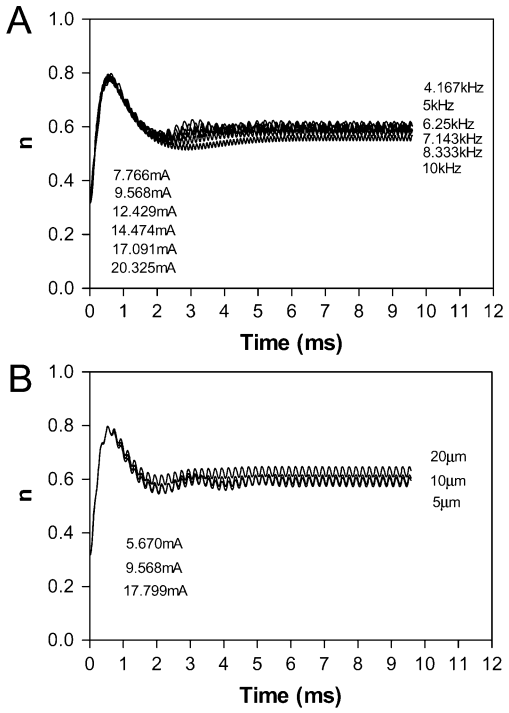

Fig. 12. Activation of the potassium channels at stimulation thresholds for inducing nerve block. (A) Different stimulation frequencies with axon diameter 10 μm. (B) Different axon diameters at a frequency 5 kHz. The intensity thresholds are also listed in the order corresponding to the frequency in (A) and the diameter in (B).

larger diameter axons have a higher activation level of potassium channels [Fig. 11(A)]. This agrees very well with the result shown in Fig. 4(B), where larger axons are blocked by lower stimulation intensities. As shown in Fig. 11 axons of diameter larger than 10 μm are blocked by stimulation intensities which correspond to an activation level of potassium channels at or above 0.6 [Fig. 11(A)]. Fig. 11(B) and (C) shows again that the sodium channels can still be activated when nerve block occurs.

Fig. 12 shows the activation of potassium channels at thresholds of nerve block. Although the intensity thresholds are different for different stimulation frequencies [Fig. 12(A)] and for different axon diameters [Fig. 12(B)], the activation levels of potassium channels at which nerve block occurs are almost the same (around 0.6). This again indicates that it is the high activation level of potassium channels that blocks nerve conduction rather than the inactivation of sodium channels.

E. Eliminating Initial Nerve Firing

The initial nerve firing shown in Fig. 2(A), (B), and (D) when the high-frequency biphasic currents are applied to nerves can be eliminated by ramping up the stimulation intensity gradually. Fig. 13 shows that the activation and inactivation of the ion channels approach their final states gradually when the stimulation intensity ramps up. This eliminates the large initial activation of sodium channels. Therefore, the initial action potential induced by applied stimulation is eliminated.

IV. Discussion

The nerve model used in this study successfully simulated the conduction block in unmyelinated axons induced by high-frequency biphasic electrical currents. This axonal block requires a stimulation frequency higher than 4 kHz (Fig. 3), otherwise repetitive nerve firing occurs [Figs. 2(C) and 3(A) and (B)]. The lowest frequency of 4 kHz to block nerve conduction was also observed on the myelinated axons of cat sciatic/peroneal nerve [11], [12], [14]. Our simulation also showed that high-frequency biphasic stimulation blocked the large axons first, and then progressively blocked the smaller axons when stimulation intensity was gradually increased (Fig. 4). This relation between nerve block and axonal diameter was also demonstrated in frog sciatic nerve using 20 kHz sinusoidal stimulation [13]. Finally, the initial axonal responses to high-frequency biphasic stimulation could be eliminated by slowly ramping up the stimulation intensity (as shown in Fig. 13) was also evident in cat sciatic nerve [14]. In summary, this study indicates that the unmyelinated axons can be blocked by high-frequency biphasic electrical currents in a similar way as myelinated axons.

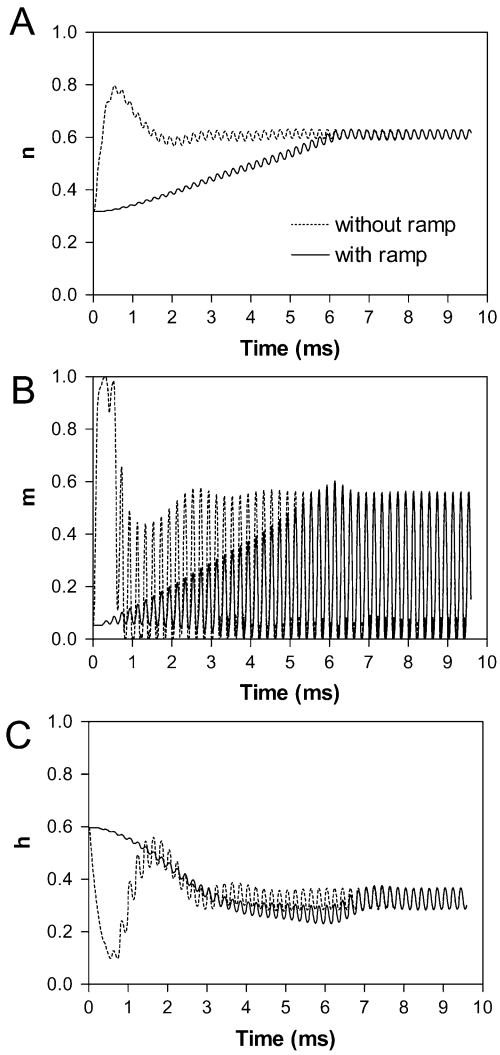

Fig. 13. Activation and inactivation of the ion channels with and without initial stimulation ramp up. (A) n—activation of K^+ channels. (B) m—activation of Na^+ channels. (C) h—inactivation of Na^+ channels. The legends in (A) are for all figures. Axon diameter: 10 μm. Stimulation frequency: 5 kHz. Stimulation intensity: 10 mA. Stimulation is gradually increased from 0 mA to 10 mA within the first 6 ms when ramp is used.

This study also predicted some new results which have not yet been shown or are difficult to show in animal experiments.

For example, increasing stimulation frequency above 4 kHz will require higher stimulation intensity to block the nerve [Fig. 4(A)]. This has not been examined in electrophysiological experiments using animals. The stimulation waveform with a fixed pulsewidth is less effective than that in which the pulsewidth changes with frequency (Fig. 5). However, only the stimulation waveform with a fixed pulsewidth was tested in animal experiments using high-frequency biphasic pulses [14]. We also discovered that the nerve block occurs right under the block electrode rather than at adjacent sites (Figs. 6 and 7), which is difficult to show in animal experiments. These new results could be a guide for future experiments on animals and also needs to be verified by animal experiments.

This simulation study suggests a possible mechanism underlying the conduction block in unmyelinated axons induced by high-frequency biphasic currents. The high activation level of potassium channels maintained by the high-frequency stimulation blocks action potential initiation and propagation (Figs. 7 and 8). Since the sodium channels can still be activated during the high-frequency stimulation (Figs. 9 –11), the potassium channels (Fig. 12) must be responsible for the conduction block. The nerve block mechanism suggested in this simulation study needs to be further confirmed by neurophysiologic experiments using animals before it can be finally accepted. It is also uncertain that this mechanism is directly applicable to the mammalian myelinated nerves where potassium currents are absent or very small [17], [18]. More evidence from either animal experiments or model analysis is needed to verify the mechanism of the conduction block in unmyelinated axons, and to discover any new mechanism in myelinated axons.

The HH model [15] was used in this study to simulate the conduction block in unmyelinated axons. The FH model [16] or other models describing mammalian axon membranes [17], [18] could also be used to replace the HH model in this study. A comparable study using other membrane models may further illustrate the mechanism of conduction block in mammalian/myelinated axons.

Only high-frequency stimulation using biphasic pulses was analyzed in this simulation study. Blocking muscle contraction by electrical stimulation of peripheral nerve using high-frequency uniphasic pulses was also reported [28]–[30]. However, the blocking mechanism for high-frequency uniphasic pulses might be different from the blocking action of high-frequency biphasic pulses. A further simulation study is needed to reveal the blocking mechanism for uniphasic pulses.

This study confirmed many known experimental phenomena, predicted some new results and suggested a possible mechanism for conduction block in unmyelinated axons induced by high-frequency biphasic currents. Understanding nerve conduction block could help in the design of better stimulation waveforms for electrical nerve block which may find many clinical applications [1]–[9].

APPENDIX

The ionic current $I_{i,n}$ at the nth segment is described as

$$I_{i,n} = g_{Na} m^3 h (V_n - V_{Na}) + g_K n^4 (V_n - V_K) + g_L (V_n - V_L)$$

where g_{Na} (120 $\mathrm{k\Omega^{-1}cm^{-2}}$), g_K (36 $\mathrm{k\Omega^{-1}cm^{-2}}$) and g_L (0.3 $\mathrm{k\Omega^{-1}cm^{-2}}$) are the maximum conductances for sodium, potassium, and leakage currents respectively; V_{Na} (115 mV), V_K (−12 mV) and V_L (10.589 mV) are reduced equilibrium membrane potentials for sodium, potassium, and leakage ions, in which the resting membrane potential V_{rest} (−70 mV) has been subtracted. m, h, and n are dimensionless variables, whose values always change between 0 and 1. m and h represent activation and inactivation of sodium channels, whereas n represents activation of potassium channels. The evolution equations for m, h, n are the following:

$$dm/dt = \alpha_m(1-m) - \beta_m m$$
$$dh/dt = \alpha_h(1-h) - \beta_h h$$
$$dn/dt = \alpha_n(1-n) - \beta_n n$$

and

$$\alpha_m = \Phi \cdot \frac{2.5 - 0.1V_n}{\exp(2.5 - 0.1V_n) - 1}$$
$$\beta_m = \Phi \cdot 4\exp\left(-\frac{V_n}{18}\right)$$
$$\alpha_h = \Phi \cdot 0.07\exp\left(-\frac{V_n}{20}\right)$$
$$\beta_h = \Phi \cdot \frac{1}{\exp(3 - 0.1V_n) + 1}$$
$$\alpha_n = \Phi \cdot \frac{0.1(1 - 0.1V_n)}{\exp(1 - 0.1V_n) - 1}$$
$$\beta_n = \Phi \cdot 0.125\exp\left(-\frac{V_n}{80}\right)$$
$$\Phi = 3^{(T-6.3)/10}$$

where T is temperature (18.5 °C). The initial values for m, h, and n (when $V_n = 0$ mV) are 0.053, 0.596, and 0.318, respectively.

REFERENCES

[1] M. Ishigooka, T. Hashimoto, I. Sasagawa, K. Izumiya, and T. Nakada, "Modulation of the urethral pressure by high-frequency block stimulus in dogs," *Eur. Urol.*, vol. 25, pp. 334–337, 1994.

[2] S. Schumacher, S. Bross, J. R. Scheepe, C. Seif, K. P. Junemann, and P. Alken, "Extradural cold block for selective neurostimulation of the bladder: Development of a new technique," *J. Urol.*, vol. 161, pp. 950–954, 1999.

[3] S. J. Tsai, H. L. Lew, E. Date, and L. I. Bih, "Treatment of detrusor-sphincter dyssynergia by pudendal nerve block in patients with spinal cord injury," *Arch. Phys. Med. Rehab.*, vol. 83, pp. 714–717, 2002.

[4] D. M. Long, "Electrical stimulation for the control of pain," *Arch. Surg.*, vol. 112, pp. 884–888, 1977.

[5] B. S. Nashold, J. L. Goldner, J. B. Mullen, and D. S. Bright, "Long-term pain control by direct peripheral-nerve stimulation," *J. Bone Joint Surg.*, vol. 64A, pp. 1–10, 1982.

[6] R. Baratta, M. Ichie, S. K. Hwang, and M. Solomonow, "Orderly stimulation of skeletal muscle motor units with tripolar nerve cuff electrode," *IEEE Trans. Biomed. Eng.*, vol. 36, no. 8, pp. 836–843, Aug. 1989.

[7] Z. P. Fang and J. T. Mortimer, "A method to effect physiological recruitment order in electrically activated muscle," *IEEE Trans. Biomed. Eng.*, vol. 38, no. 2, pp. 175–179, Feb. 1991.

[8] C. Tai and D. Jiang, "Selective stimulation of smaller fibers in a compound nerve trunk with single cathode by rectangular current pulses," *IEEE Trans. Biomed. Eng.*, vol. 41, no. 3, pp. 286–291, Mar. 1994.

[9] W. F. Agnew and D. B. McCreery, *Neural Prostheses: Fundamental Studies*. Englewood Cliffs, NJ: Prentice-Hall, 1990.

[10] M. Cattell and R. W. Gerard, "The "inhibitory" effect of high-frequency stimulation and the excitation state of nerve," *J. Physiol. (Lond.)*, vol. 83, pp. 407–415, 1935.

[11] J. Reboul and A. Rosenblueth, "The action of alternating currents upon the electrical excitability of nerve," *Am. J. Physiol.*, vol. 125, pp. 205–215, 1939.
[12] A. Rosenblueth and J. Reboul, "The blocking and deblocking effects of alternating currents on nerve," *Am. J. Physiol.*, vol. 125, pp. 251–264, 1939.
[13] J. A. Tanner, "Reversible blocking of nerve conduction by alternating-current excitation," *Nature*, vol. 195, pp. 712–713, 1962.
[14] B. R. Bowman and D. R. McNeal, "Response of single alpha motoneurons to high-frequency pulse train: Firing behavior and conduction block phenomenon," *Appl. Neurophysiol.*, vol. 49, pp. 121–138, 1986.
[15] A. L. Hodgkin and A. F. Huxley, "A quantitative description of membrane current and its application to conduction and excitation in nerve," *J. Physiol. (Lond.)*, vol. 117, pp. 500–544, 1952.
[16] B. Frankenhaeuser and A. F. Huxley, "The action potential in the myelinated nerve fiber of *Xenopus Laevis* as computed on the basis of voltage clamp data," *J. Physiol. (Lond.)*, vol. 171, pp. 302–315, 1964.
[17] S. Y. Chiu, J. M. Ritchie, R. B. Rogart, and D. Stagg, "A quantitative description of membrane currents in rabbit myelinated nerve," *J. Physiol. (Lond.)*, vol. 292, pp. 149–166, 1979.
[18] J. R. Schwarz and G. Eikhof, "Na currents and action potentials in rat myelinated nerve fibers at 20 and 37 °C," *Pflugers Arch.*, vol. 409, pp. 569–577, 1987.
[19] D. R. McNeal, "Analysis of a model for excitation of myelinated nerve," *IEEE Trans. Biomed. Eng.*, vol. BME-23, pp. 329–337, 1976.
[20] J. P. Reilly, V. T. Freeman, and W. D. Larkin, "Sensory effects of transient electrical stimulation—Evaluation with a neuroelectric model," *IEEE Trans. Biomed. Eng.*, vol. BME-32, pp. 1001–1011, 1985.
[21] F. Rattay, "High frequency electrostimulation of excitable cells," *J. Theor. Biol.*, vol. 123, pp. 45–54, 1986.
[22] P. H. Veltink, J. A. V. Alste, and H. B. K. Boom, "Simulation of intrafascicular and extraneural nerve stimulation," *IEEE Trans. Biomed. Eng.*, vol. 35, no. 1, pp. 69–75, Jan. 1988.
[23] K. W. Altman and R. Plonsey, "Point source nerve bundle stimulation: Effects of fiber diameter and depth on simulated excitation," *IEEE Trans. Biomed. Eng.*, vol. 37, no. 7, pp. 688–698, Jul. 1990.
[24] F. Rattay and M. Aberham, "Modeling axon membranes for functional electrical stimulation," *IEEE Trans. Biomed. Eng.*, vol. 40, no. 12, pp. 1201–1209, Dec. 1993.
[25] J. H. M. Frijns, J. Mooij, and J. H. ten Kate, "A quantitative approach to modeling mammalian myelinated nerve fibers for electrical prosthesis design," *IEEE Trans. Biomed. Eng.*, vol. 41, no. 6, pp. 556–566, Jun. 1994.
[26] C. C. McIntyre, A. G. Richardson, and W. M. Grill, "Modeling the excitability of mammalian nerve fibers: Influence of afterpotentials on the recovery cycle," *J. Neurophysiol.*, vol. 87, pp. 995–1006, 2002.
[27] J. W. Cooley and F. A. Dodge Jr., "Digital computer solutions for excitation and propagation of the nerve impulse," *Biophys. J.*, vol. 6, pp. 583–599, 1966.
[28] M. Solomonow, E. Eldred, J. Lyman, and J. Foster, "Control of muscle contractile force through indirect high-frequency stimulation," *Am. J. Physical Med.*, vol. 62, pp. 71–82, 1983.
[29] ——, "Fatigue considerations of muscle contractile force during high-frequency stimulation," *Am. J. Physical Med.*, vol. 62, pp. 117–122, 1983.
[30] M. Solomonow, "External control of the neuromuscular system," *IEEE Trans. Biomed. Eng.*, vol. BME-31, pp. 752–763, 1984.

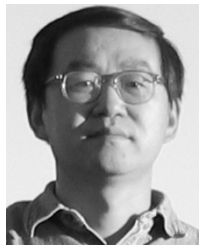

Changfeng Tai (M'97, SM'01) received the B.S., M.S., and Ph.D. degrees in biomedical engineering from the Xi'an Jiaotong University, China, in 1986, 1989, and 1992, respectively.

After his postdoctoral training in the Department of Rehabilitation Science and Technology at the University of Pittsburgh, Pittsburgh, PA, he joined the Department of Pharmacology at the same University, where he is presently an Assistant Professor. His research interests include functional neuromuscular stimulation to restore micturiton and motor functions after spinal cord injury, model analysis of nerve stimulation, biomedical signal processing, and neural control of micturition.

Dr. Tai is member of the Society for Neuroscience.

William C. de Groat received the B.S. degree in pharmacy and the M.S. degree from the Philadelphia College of Pharmacy and Sciences, Philadelphia, PA, in 1960 and 1962. He received the Ph.D. degree in pharmacology from the Department of Pharmacology at the University of Pennsylvania Medical School, Philadelphia, in 1965.

After his postdoctoral work in neurophysiology in the Department of Physiology of the John Curtin School of Medical Research, Canberra, Australia, he joined the Department of Pharmacology at the University of Pittsburgh School of Medicine, Pittsburgh, PA, in 1968, where he is presently a Professor of Pharmacology. His laboratory is studying the organization of the lumbosacral autonomic reflex pathways in a variety of animal models. He is interested in the identity of the neurotransmitters at peripheral ganglionic and central autonomic synapses, the central mechanisms involved in viscerosomatic integration, the maturation of autonomic reflexes during postnatal development, the mechanisms underlying the recovery of function following spinal cord injury, and visceral nociceptive pathways.

James R. Roppolo reveived the B.S. degree in pharmacy from the University of Pittsburgh, Pittsburgh, PA, in 1965. He received the Ph.D. degree in neuropharmacology from the Department of Pharmacology at the University of Michigan School of Medicine, Ann Arbor, MI, in 1970.

After his postdoctoral work in neuropharmacology and neurophysiology in the Department of Pharmacology at the University of Pittsburgh School of Medicine, Pittsburgh, PA, he joined the department as a faculty member and is presently an Assistant Professor. His research interests are centered around the central antonomic pathways which control bladder, colon, and sexual functions, as well as the somatic motor pathways which produce limb movements. Of particular interest is the restoration of autonomic and motor function following spinal cord injury.

Dr. Roppolo is member of Society for Neuroscience.